Atmospheric Oxidation Mechanism of *p*-Xylene: A Density Functional Theory Study

Jiwen Fan and Renyi Zhang*

Department of Atmospheric Sciences, Texas A&M University, College Station, Texas 77843

Received: March 20, 2006; In Final Form: April 19, 2006

We report an investigation of the mechanistic features of OH-initiated oxidation reactions of *p*-xylene using density function theory (DFT). Reaction energies for the formation of the aromatic intermediate radicals have been obtained to determine their relative stability and reversibility, and their activation barriers have been analyzed to assess the energetically favorable pathways to propagate the *p*-xylene oxidation. OH addition is predicted to occur dominantly at the ortho position, with branching ratios of 0.8 and 0.2 for ortho and ipso additions, respectively, and the calculated overall rate constant is in agreement with available experimental studies. Under atmospheric conditions, the *p*-xylene peroxy radicals arising from initial OH and subsequent O_2 additions to the ring are shown to cyclize to form bicyclic radicals, rather than to react with NO to lead to ozone formation. With relatively low barriers, isomerization of the *p*-xylene bicyclic radicals to more stable epoxide radicals likely occurs, competing with O_2 addition to form bicyclic peroxy radicals. The study provides thermochemical and kinetic data for assessment of the photochemical production potential of ozone and formation of toxic products and secondary organic aerosol from *p*-xylene oxidation.

1. Introduction

Aromatic compounds constitute 30–40% of hydrocarbon mass emitted into urban atmospheres and represent a significant source of urban ozone, photochemical smog and secondary organic aerosol (SOA) formation.[1,2] The SOA impacts human health and the climate.[3] Also, the likely formation of toxic epoxide products from aromatic oxidation is of considerable concern.[4] The aromatics are emitted into the atmosphere via automobile emissions and solvent use.[2] Although toluene is usually the most prominent aromatic compounds, the combined xylene isomers have contributed similar mass in most studies.[5–7] Xylene is one of the top 30 chemicals produced in the United States in terms of volume. Levels of xylenes measured in the air of industrial areas and cities of the United States range from 1 to 88 parts of xylenes per billion parts of air.[8]

The reaction of aromatic hydrocarbons with hydroxyl radicals (OH) represents the major atmospheric loss process during daylight hours. Hydroxyl radicals react with aromatic compounds by abstracting hydrogen atoms from the alkyl group or by adding to the aromatic ring.[1,9] H atom abstraction is relatively minor for xylene isomers (less than 10%).[1,10,11] The addition of OH to the xylene ring forms OH–xylene adducts. Under atmospheric conditions, O_2 is expected to rapidly add to the OH–xylene adduct, forming primary peroxy radicals.[12,13] The fate of the xylene peroxy radicals is governed by competition between reaction with NO to form alkoxy radicals and cyclization to form bicyclic radicals. For *p*-xylene–OH–O_2 peroxy radicals, the cyclization reaction is expected to be more important than reaction with NO at typical atmospheric levels, on the basis of a theoretical study.[13] The large yields of hexenedione, glyoxal, and methylglyoxal detected in the work by Smith et al. also support the preference of cyclization reaction to form bicyclic radicals.[1] Volkamer et al. also identified cyclization as the major pathway for the oxidation of *p*-xylene.[14] The bicyclic radicals then undergo unimolecular rearrangement to form epoxide

radicals or bimolecular reaction with O_2 to form (secondary) bicyclic peroxy radicals. The mechanistic complexity of the *p*-xylene oxidation further arises from multiple isomeric pathways at each reaction stage. Initial OH addition to *p*-xylene results in two distinct structural *p*-xylene–OH adduct isomers (i.e., ortho and ispo). Subsequent reactions of the *p*-xylene–OH adducts with O_2 and cyclization of the peroxy radicals also incur additional isomeric branching. Scheme 1 illustrates the likely pathways of *p*-xylene oxidation initiated by OH.

Experimental studies have investigated the temperature- and pressure-dependent rate constant of the initial *p*-xylene–OH reaction.[11,12,15,16] The room-temperature rate constant for *p*-xylene reported by Bandow and Washida is 1.4×10^{-11} cm³ molecule⁻¹ s⁻¹ with an uncertainty factor about ±2 at 300 K and 1 atm.[10,15] There has been considerable experimental work on the products from the reactions of OH with *p*-xylene. Environmental chamber studies have identified several major products consisting of both ring-retaining and fragmentation compounds.[1,2,4,14–18] The experimental work carried out by Volkamer et al. reported a significant yield (about 40 ± 10%) of glyoxal and indicated that the ring-cleavage pathway involving the bicyclic peroxy radical represents the major pathway for the oxidation of *p*-xylene initiated by OH.[14] Experimental studies detected the large quantities of *E*- and *Z*-isomers of hex-3-ene-2,5-dione, qualitatively consistent with the work of Smith et al., in which both isomers were identified as primary products, with the yields of 18% for *Z*-isomer and 5% for *E*-isomer.[1,2] Smith et al. also identified another unsaturated dicarbonyl product from the ring fragmentation of *p*-xylene, i.e., 2-methyl-2-butenedial, with a yield of 7%.[1]

At present, however, the detailed mechanism of *p*-xylene oxidation following the initial OH attack remain highly uncertain. Most of the aromatic intermediate radicals have not yet been detected directly in the gas phase. In previous experimental product studies of xylenes, typically less than 65% of the reacted carbon has been identified as products.[1,14–20] Interpretation of the identified reaction products is hindered because of the existence of multiple reaction pathways and steps. On the other

Atmospheric Oxidation Mechanism of *p*-Xylene

J. Phys. Chem. A, Vol. 110, No. 24, 2006 **7729**

SCHEME 1: Mechanistic Diagram of the *p*-Xylene−OH Reaction System
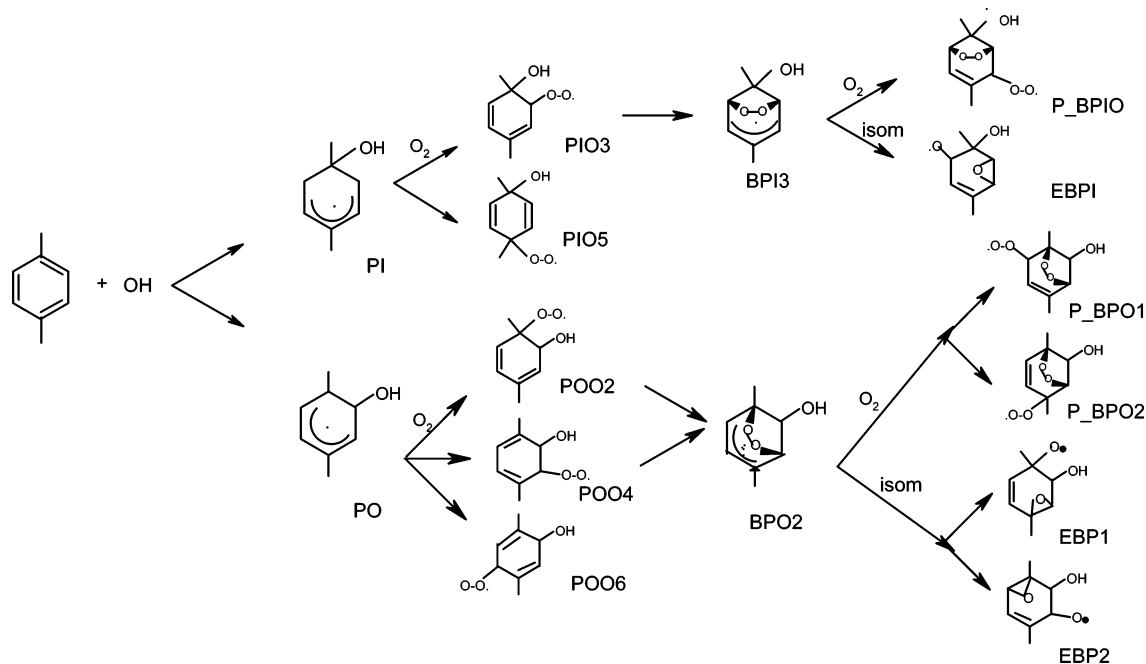
hand, theoretical studies can be extremely useful in evaluating the possible mechanisms of the aromatic oxidation. In this work, we present a comprehensive theoretical investigation of the reaction of OH with *p*-xylene and the subsequent reactions, including the formation of aromatic peroxy, bicyclic, epoxide, and bicyclic peroxy radicals. We have calculated the rate constants and isomeric branching of the reactions of those aromatic reactions. Reaction energies for the formation of the aromatic radicals have been obtained to determine their relative stability and reversibility, and the activation barriers have been analyzed to assess the energetically favorable pathways to propagate the *p*-xylene oxidation.

2. Theoretical Method

The theoretical computations were performed on an SGI Origin 3800 supercomputer using the GAUSSIAN 98 software package, similar to those in our previous studies for OH-initiated oxidation of toluene.[21,22] Briefly, all radicals were treated with the unrestricted Hartree−Fock (UHF) formulation. Geometry optimization was executed using Becke's three parameter hybrid method employing the LYP correction function (B3LYP) in conjunction with the split valence polarized basis set 6-31G(d,p).

Rate constants of unimolecular (k_{uni}) and bimolecular (k_b) reactions of the aromatic intermediate radicals were calculated using classic transition state theory (TST). The high-pressure limit unimolecular rate constant is expressed by[23−25]

$$k_{uni} = \frac{kT}{h}\frac{Q^{\ddagger}_{AB}}{Q_{AB}}\exp\left(-\frac{\Delta E}{kT}\right) \qquad (1)$$

where $Q^{\ddagger}_{AB}$ is the partition function of the transition state with the vibrational frequency corresponding to the reaction coordinate removed, Q_{AB} is the partition function of the reactant, and E_a is the zero-point corrected activation energy. The association rate is related to the dissociation rate by the equilibrium constant (K):[23−25]

$$\frac{k_{rec}}{k_{uni}} = K_{eq} = \frac{Q_{AB}}{Q_A Q_B}\exp\left(\frac{D_0}{kT}\right) \qquad (2)$$

where Q_{AB} is the partition function of the dissociating species, Q_A and Q_B are the partition functions of the fragmentation products, and D_0 is the zero-point corrected binding energy.

3. Result and Discussion

3.1. *p*-Xylene━OH Adducts. OH addition to *p*-xylene forms two possible isomers of *p*-xylene−OH adducts, i.e., ipso and ortho isomers (Scheme 1). Figure 1 depicts the optimized geometries of the two adducts and their corresponding transition states obtained at the B3LYP/6-31G(d,p) level of theory. Addition of OH to *p*-xylene leads to a lengthening of C−C bonds adjunct to the site of addition. For the ipso isomer (PI), the C−C bond lengths are increased by 0.10 Å between C1−C2 and C1−C6 and by 0.02 Å between C1 and C7 (the methyl carbon). The increased C−C bond length adjacent to the OH addition site reflects an increased σ character, as electron density is transferred to the newly formed C−O bonds. Similar C−C bonding characteristics are observed for ortho isomer (PO), the bond lengths are increased by 0.11 Å between C1−C2 and C2−C3. The C−O bond distance is 1.45 Å for both isomers. At the transition states, the C−O distance is 2.07 Å for PI and 2.06 Å for PO. A comparison of the structures of *p*-xylene, the adduct isomers, and the transition states clearly reveals the intermediate features in the transition state structures.

Spin contamination with the B3LYP optimized geometries of the two adduct isomers is minimal. The calculated spin eigenvalues, $\langle S^{**}2\rangle$, are 0.786 and 0.787 for PI and PO, respectively. After the $S + 1$ component is annihilated, the values of $\langle S^{**}2\rangle$ are reduced to 0.751 for two isomers, nearly identical to the exact value of a pure doublet. This implies that contamination of the unrestricted Hartree−Fock wave function from higher spin states is negligible for both isomers.

Results of calculated zero-point corrected reaction binding energies (RE) and the activation energies (E_a) at the B3LYP/6-31G(d,p) level for *p*-xylene−OH adduct formation are provided in Table 1. The reaction energies for PI and PO are very close, with the values of −17.2 and −17.8 kcal mol⁻¹, respectively. The activation energy for PO is about 1.0 kcal mol⁻¹ less than that for PI. For both OH addition pathways,
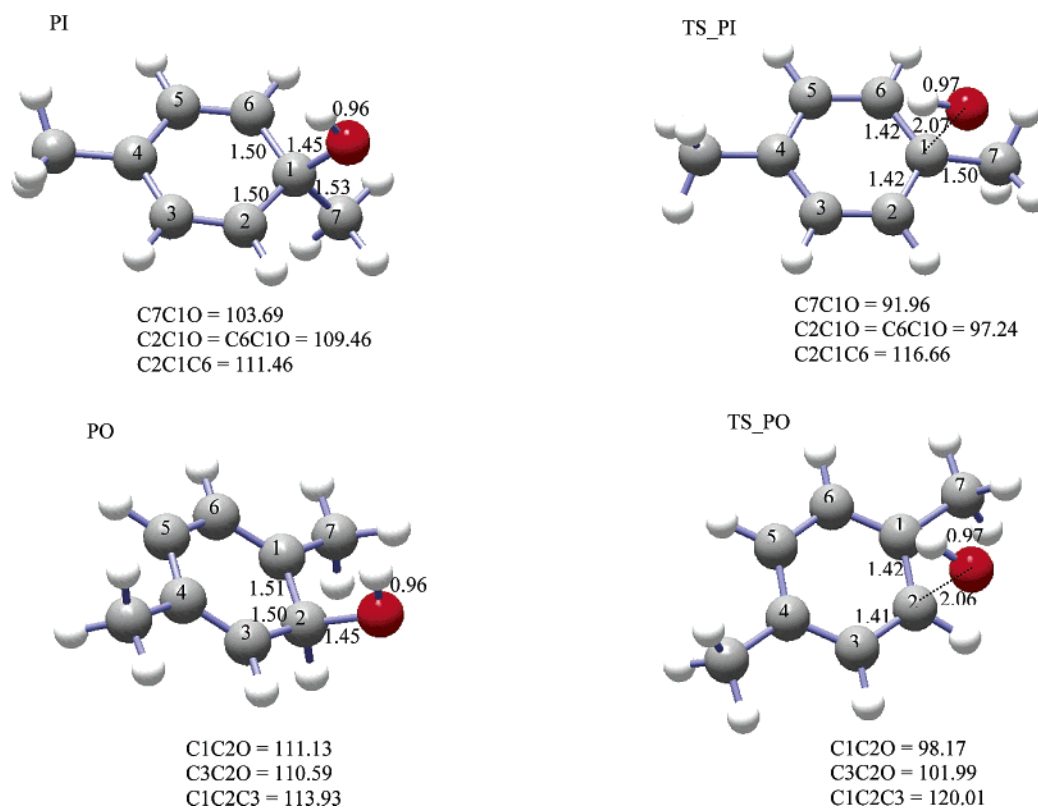
PI

C7C1O = 103.69
C2C1O = C6C1O = 109.46
C2C1C6 = 111.46

TS_PI

C7C1O = 91.96
C2C1O = C6C1O = 97.24
C2C1C6 = 116.66

PO

C1C2O = 111.13
C3C2O = 110.59
C1C2C3 = 113.93

TS_PO

C1C2O = 98.17
C3C2O = 101.99
C1C2C3 = 120.01

Figure 1. Optimized geometries of *p*-xylene−OH adducts and their corresponding transition states at the B3LYP/6-31G(d,p) level of theory.

TABLE 1: Zero-Point Corrected Reaction Energies, Activation Energies, High-Pressure Rate Constants, and Branching Ratios of *p*-Xylene−OH Reaction

species	RE (kcal mol^{-1})	E_a (kcal mol^{-1})	k_{rec} (cm^3 mol^{-1} s^{-1})	k_{uni} (s^{-1})	K	R	k(tot) (cm^3 mol^{-1} s^{-1})
PI	−17.22	−2.49	1.8×10^{-12}	2.0×10^2	2.2×10^5	0.20	
PO	−17.79	−3.48	7.4×10^{-12}	6.9×10^2	2.7×10^5	0.80	9.24×10^{-12}

the activation energies predicted are negative. On the basis of the presently obtained activation energies and the transition state theory (TST), the high-pressure rate constants for the formation of the *p*-xylene−OH adduct radicals (k_{rec}) are calculated. As shown in Table 1, the calculated high-pressure rate constants for PI and PO at the B3LYP/6-31G(d,p) level are 1.8×10^{-12} cm^3 molecule^{-1} s^{-1} and 7.4×10^{-12} cm^3 molecule^{-1} s^{-1}, respectively. The resulted combined rate constant for OH addition to *p*-xylene is 9.2×10^{-12} cm^3 molecule^{-1} s^{-1}. Assuming the branching ratio of the hydrogen abstraction reaction is 0.08,[20] the overall rate constant of OH reaction with *p*-xylene is 1.0×10^{-11} cm^3 molecule^{-1} s^{-1}, in agreement with the recommended value of 1.4×10^{-11} cm^3 molecule^{-1} s^{-1} at 300 K and one atm (ref 20), considering the combined uncertainties of experimental and theoretical studies. The decomposition rate constants for *p*-xylene−OH adduct isomers are also calculated, which are 2.0×10^2 and 6.9×10^2 s^{-1} for PI and PO, respectively (Table 1). The branching ratio for each OH addition pathway (R) is determined on the basis of the calculated high-pressure rate constants and also provided in Table 1. For the formation of PI and PO, the branching ratios are 0.20 and 0.80, respectively, suggesting a strong preference for the ortho addition of OH to *p*-xylene.

3.2. *p*-Xylene—OH—O₂ Peroxy Radicals. O$_2$ addition to the ipso *p*-xylene−OH adduct forms two possible structural isomers of the peroxy radicals, i.e., PIO3 and PIO5 (Scheme 1). Oxygen addition to the ortho *p*-xylene−OH adduct results in three plausible peroxy radical isomers, i.e., POO2, POO4 and POO6. Figure 2 depicts the optimized geometries of the

lowest-energy conformations of the peroxy radicals obtained using B3LYP/6-31G(d,p). For the peroxy radicals, the energetically favorable conformation corresponds to O$_2$ addition on the same side of the benzene ring as the hydroxyl group, resulting in a stabilization of more than 5 kcal mol^{-1}. The C−C bond lengths adjacent to the site of O$_2$ addition are increased, as electron density in the π bond is transferred to the newly formed C−O bonds. Figure 2 shows that there exists intramolecular hydrogen binding in the peroxy radicals. It involves interaction between the terminal oxygen of the peroxy group and the hydrogen of the OH group, forming a six-membered ring. The distance of intramolecular hydrogen binding ranges from 1.86 to 2.34 Å, with the latter value corresponding to rather weak hydrogen binding. Compared with the *p*-xylene−OH adduct geometries shown in Figure 1, the addition of O$_2$ to the *p*-xylene−OH adduct results in a shortening of the C−O(H) bond. For peroxy radicals PIO3, POO2, and POO4, in which the intramolecular hydrogen binding is stronger, the reduced length of the C−O(H) bonds is 0.04 Å. The C−O(H) bond length for PIO5 and POO6 is reduced much less, only 0.01− 0.02 Å, corresponding to rather weak intramolecular hydrogen binding.

The transition state (TS) structures for the formation of peroxy radicals are illustrated in Figure 3. The C−O bond lengths at the transition states range from 2.14 to 2.20 Å. The intramolecular hydrogen binding also exists in the TS structures. The hydrogen bond lengths are between 1.87 and 2.24 Å. Note that the hydrogen bond in the ts_POO2 goes to the neighboring methyl group, due to the interaction of the lone pairs between
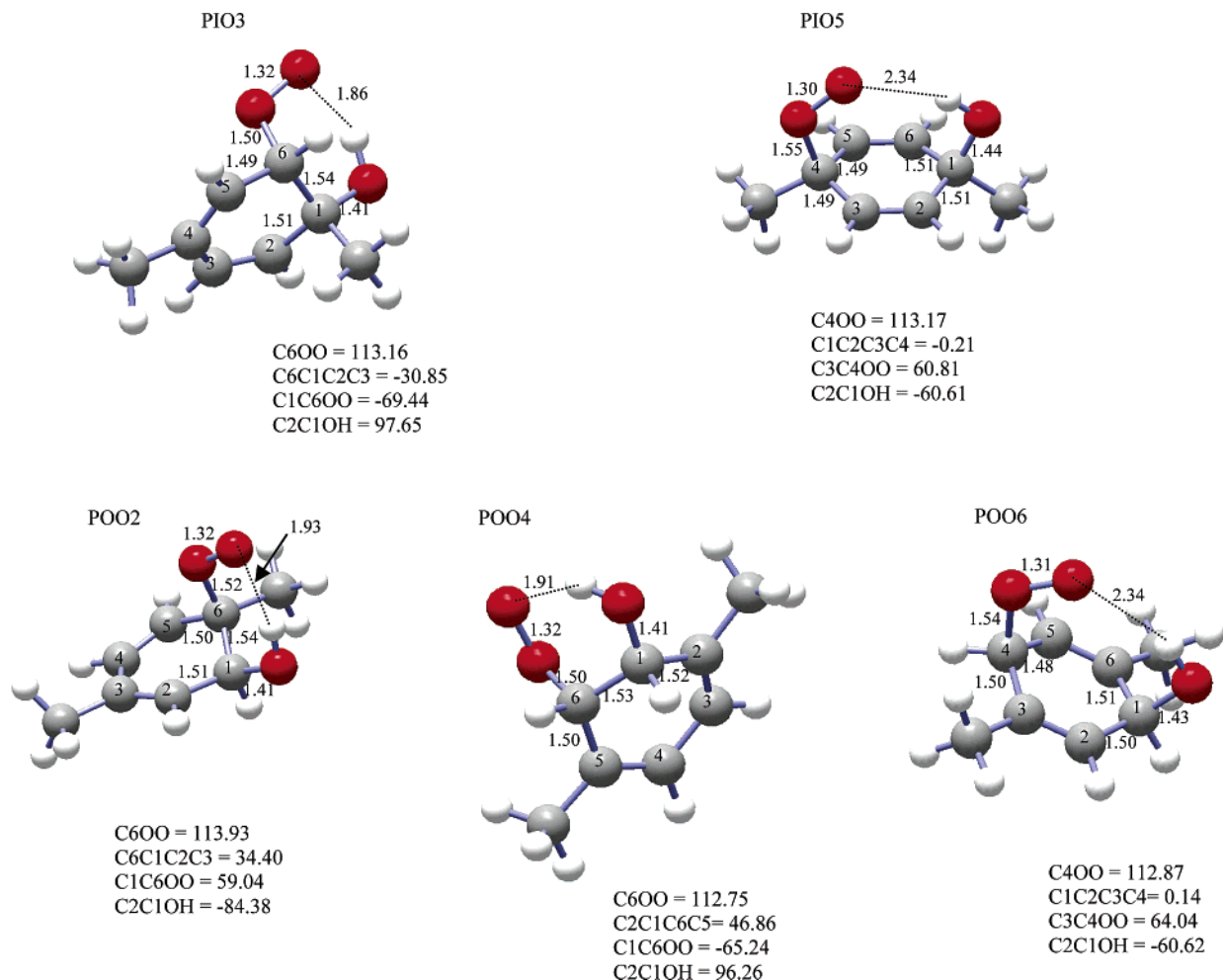
Atmospheric Oxidation Mechanism of *p*-Xylene

J. Phys. Chem. A, Vol. 110, No. 24, 2006 **7731**

Figure 2. Optimized geometries of primary peroxy radicals at the B3LYP/6-31G(d,p) level of theory.

the oxygen atom in the peroxy group and the hydrogen atom in the methyl group. The oxygen bond rotates to shorten the distance between O and H in the methyl group. On the other hand, the distance between O atom in the peroxy group and the H atom in the hydroxyl group is 2.51 Å.

Zero-point corrected reaction energies for the formation of the peroxy radicals are listed in Table 2. Addition of O_2 to *p*-xylene−OH adducts leads to formation of peroxy radicals. The binding energies of the peroxy radicals range from 4.5 to 7.1 kcal mol^{-1}. For the ortho *p*-xylene−OH adduct, O_2 addition at C6 of the aromatic ring represents the most stable isomer (POO4). It is clear that hydrogen binding plays a role in stabilizing the peroxy radicals. The POO4 has the strongest hydrogen binding among the peroxy radicals formed from ortho *p*-xylene−OH adduct, with a hydrogen bond length of 1.91Å.

The activation energies to form the peroxy radicals are also included in Table 2. The activation barrier is about 5 kcal mol^{-1} for PIO3, but is slightly negative for PIO5. The activation barriers of O_2 addition to the ortho *p*-xylene−OH adduct are less than 5 kcal mol^{-1}; POO6 also has a negative activation energy which is similar to PIO5. It is interesting to note that, although the peroxy radical POO4 represents the most stable form for O_2 addition to the ortho *p*-xylene−OH adduct, its activation energy is higher than those of POO2 and POO6.

We calculated the high-pressure limit rate constants of O_2 addition to the *p*-xylene−OH adducts, using the classic TST and the structures and energies obtained with B3LYP/6-31G-(d,p). As presented in Table 3, the calculated rate constants range from 10^{-14} to 10^{-18} cm^3 molecule^{-1} s^{-1}, showing distinct

kinetics for the isomers of the peroxy radicals. For the ipso *p*-xylene−OH adduct, O_2 addition occurs with the rate constants of 1.1×10^{-18} and 8.2×10^{-15} cm^3 molecule^{-1} s^{-1} for PIO3 and PIO5, respectively. The formation of PIO5 is much faster than PIO3 since its activation energy is much lower. For O_2 addition to the ortho *p*-xylene−OH adduct, the rate constants for POO2, POO4, and POO6 are 7.6×10^{-17}, 2.7×10^{-17}, and 3.2×10^{-14} cm^3 molecule^{-1} s^{-1}, respectively. The formation of POO6 is much faster than other two, because of the much lower activation energy.

Because of the relatively small binding energies of the peroxy radicals, the *p*-xylene−OH adducts reaction with O_2 proceeds reversibly, and the equilibrium favors peroxy radical decomposition since the equilibrium constants (*K*) for the reactions of formation of the peroxy radicals are small (Table 3). The close relative stability and reversibility of the peroxy radicals suggest that all isomers of the peroxy radicals are likely to form. The relative stability and activation barriers of the peroxy radicals, however, have little effect on isomeric branching, since propagation of the *p*-xylene oxidation is largely determined by the exit channel of the peroxy radicals. The steady-state concentrations of the peroxy radicals are determined by recombination of the adduct with O_2, dissociation of the peroxy radicals, and the exit channel of the peroxy radicals, that is, reaction with NO to form alkoxy radicals, rearrangement to form bridged bicyclic radicals, or H-abstraction to form phenols.

3.3. Bicyclic Radicals. For the ipso OH addition, the peroxy radical PIO3 likely cyclizes to form a stable bridged bicyclic radical BPI3. For the ortho OH addition, the peroxy radicals
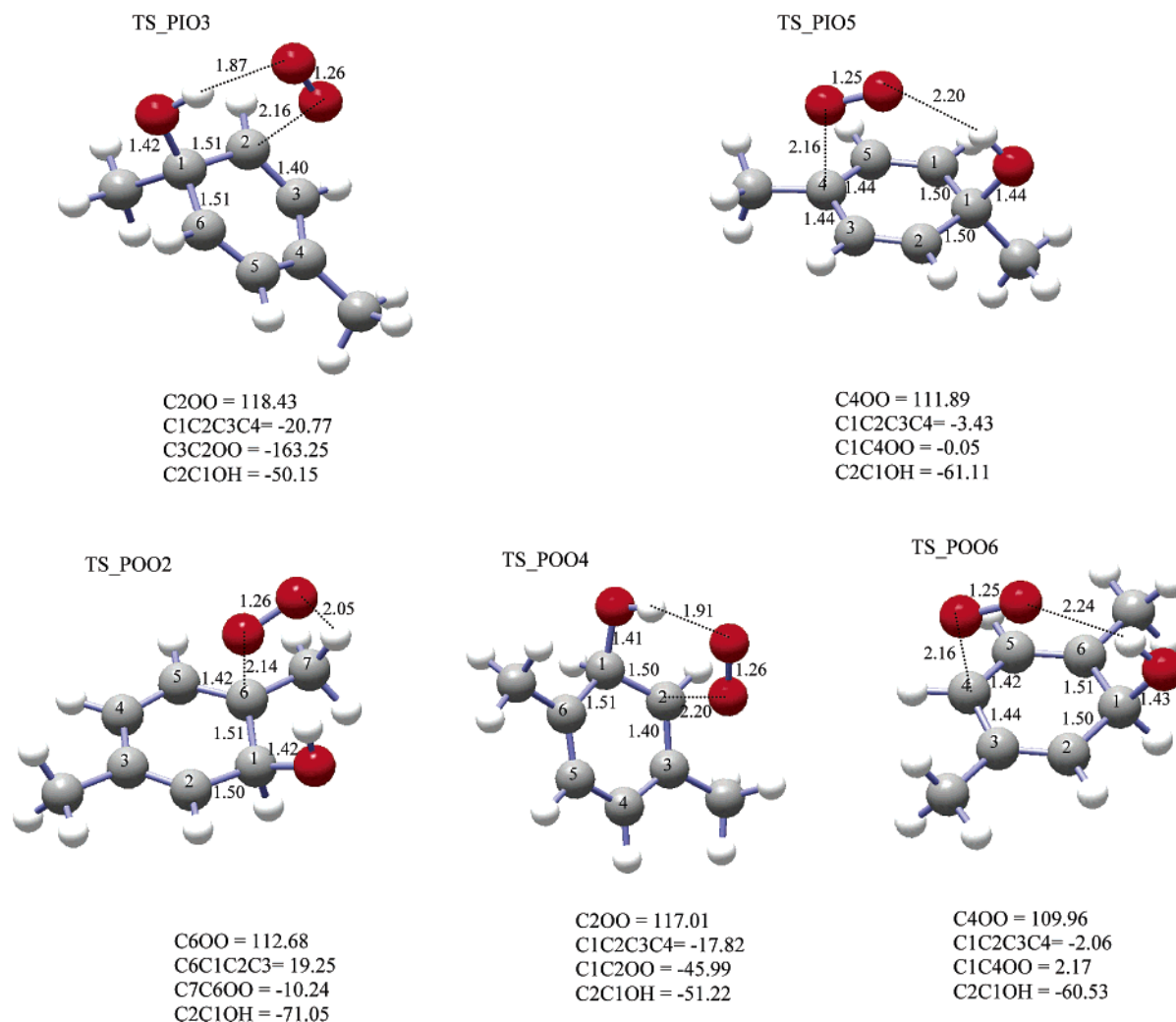
Figure 3. Transition states of primary peroxy radicals at the B3LYP/6-31G(d,p) level of theory.

TABLE 2: Zero-Point Corrected Reaction Energies (RE in kcal mol^{-1}) and Activation Energies (E_a in kcal mol^{-1}) for the *p*-Xylene−OH−O$_2$ Reaction System

type	reaction	RE	E_a	type	reaction	RE	E_a
ipso	PI + O$_2$ → PIO3	−4.87	5.03	ortho	PO + O$_2$ → POO2	−4.98	2.98
	PI + O$_2$ → PIO5	−4.5	−0.5		PO + O$_2$ → POO4	−7.05	4.18
	PIO3 → BPI3	−6.79	10.76		PO + O$_2$ → POO6	−5.07	−0.51
	BPI3 + O$_2$ → EBPI	−17.26	8.77		POO2 → BPO2 (a)	−8.76	9.07
	BPI3 + O$_2$ → P_BPIO	−14.17	2.40		POO4 → BPO2 (b)	−6.69	11.14
					BPO2 → EBP1	−14.81	6.93
					BPO2 → EBP2	−17.02	6.93
					BPO2 + O$_2$ → P_BPO1	−13.29	0.19
					BPO2 + O$_2$ → P_BPO2	−13.07	−0.71

POO2 and POO4 undergo cyclization to form an identical stable bicyclic radical BPO2. Cyclization from other peroxy radicals cannot form stable bicyclic radicals.[21] The high stability of BPI3 and BPO2 is explained since both structures possess a delocalized allyl system. Figure 4 presents the equilibrium structures and transition states of bicyclic radicals BPI3 and BPO2. For BPI3, the two C−O bonds on the ring have the same bond length of 1.45 Å. For BPO2, the C−O bonds on the ring are 1.45 and 1.46 Å. The distances for C−O closure at the transition states are 2.02 Å for both radicals. The TS structures leading to BPO2 formation from POO2 and POO4 are the same. Also, the stabilization energies for POO2 and POO4 are identical, leading to the same activation energies for BPO2 formation from POO2 and POO4. However, the detailed PES around the TS regions may be very different for both pathways. The reaction and activation energies for isomerization of peroxy to bicyclic

radicals are presented in Table 2. The potential energy surface (PES) of isomerization from the peroxy to bicyclic radical is illustrated in Figure 5. Isomerization of PIO3 to BPI3 is exothermic by about 7 kcal mol^{-1} and occurs with an activation barrier of about 11 kcal mol^{-1}. The exothermicity for BPO2 from POO2 is about 2 kcal mol^{-1} more than that from POO4, and the activation barrier is about 2 kcal mol^{-1} less. Andino et al.[13] calculated a barrier height of 12.1 kcal mol^{-1} for the formation of the bicyclic radical of *p*-xylene employing UHF/PM3 methods for geometry optimizations followed by a single-point calculation at the B3LYP/6-31G(d,p) level of theory, only slightly higher than our calculations.

The calculated unimolecular rate constants of bicyclic reactions at the B3LYP/6-31G(d,p) level of theory are also showed in Table 3. Unimolecular formation of the bicyclic radical BPI3 has a rate of 1.9×10^4 s^{-1}. The rate constants for isomerization

Atmospheric Oxidation Mechanism of *p*-Xylene

J. Phys. Chem. A, Vol. 110, No. 24, 2006 **7733**

TABLE 3: Calculated High-Pressure Limit Rate Constants of Intermediate Radicals for the *p*-Xylene−OH−O₂ Reaction System at 300 K[a]

species	k	k^{-1}	K	species	k	k^{-1}	K
PIO3	1.1×10^{-18}	1.3×10^{6}	2.1×10^{-5}	POO2	7.6×10^{-17}	3.5×10^{7}	5.3×10^{-5}
PIO5	8.2×10^{-15}	2.1×10^{10}	9.4×10^{-6}	POO4	2.7×10^{-17}	2.2×10^{5}	2.9×10^{-3}
BPI3	1.9×10^{4}	3.7×10^{-1}	5.1×10^{4}	POO6	3.2×10^{-14}	7.5×10^{9}	1.1×10^{-4}
EBPI	1.9×10^{6}	7.9×10^{-7}	2.4×10^{12}	BPO2 (a)	5.5×10^{6}	6.3	8.8×10^{5}
P_BPIO	2.3×10^{-15}	1.3×10^{2}	4.4×10^{2}	BPO2 (b)	6.9×10^{4}	4.3	1.6×10^{4}
				EBP1	4.5×10^{7}	8.0×10^{-4}	5.6×10^{10}
				EBP2	4.5×10^{7}	1.4×10^{-5}	3.2×10^{12}
				P_BPO1	2.2×10^{-14}	5.1×10^{3}	1.11×10^{2}
				P_BPO2	9.0×10^{-14}	3.5×10^{4}	6.3×10^{1}

[a] Unimolecular rate constants are in s⁻¹, and bimolecular rate constants are in cm³ molecule⁻¹ s⁻¹. Equilibrium constants K are dimensionless.
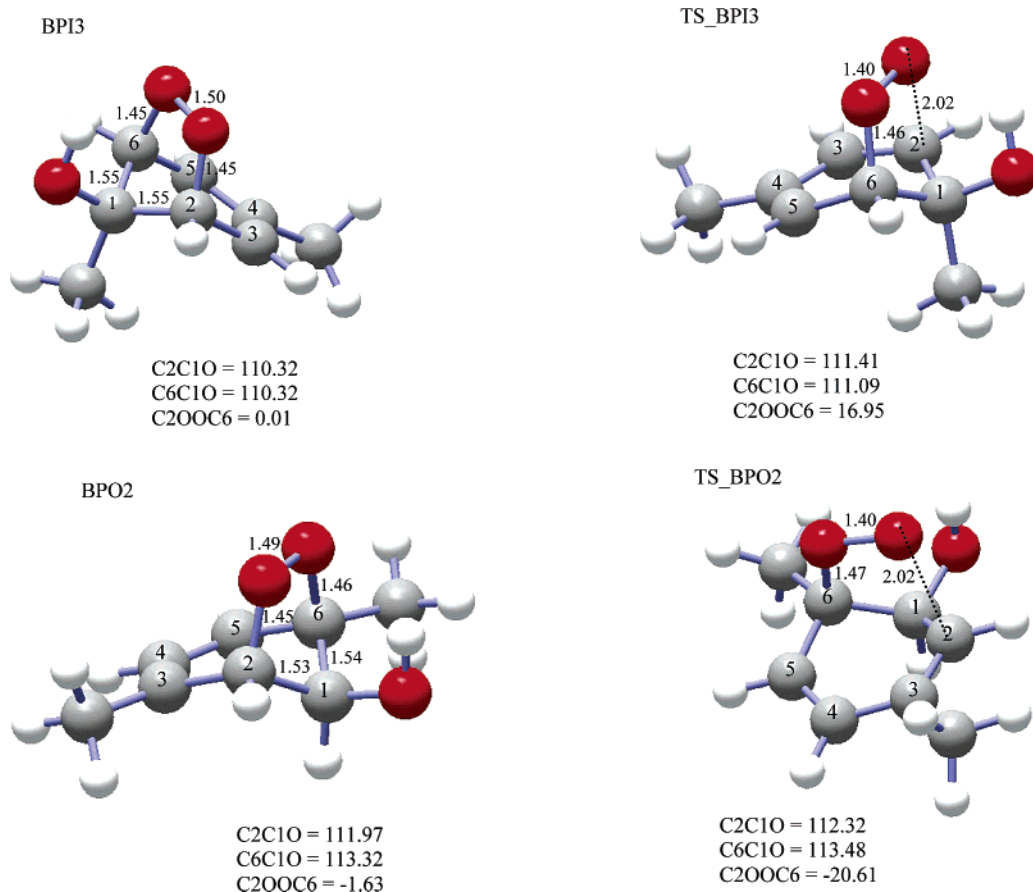
Figure 4. Optimized geometries of bicyclic radicals and their corresponding transition states at the B3LYP/6-31G(d,p) level of theory.

of POO2 and POO4 to BPO2 are 5.5×10^{6} and 6.9×10^{4} s⁻¹, respectively. The reversible rate constants are small, indicating that bicyclic isomerization of the peroxy radicals is almost irreversible (Table 3). The calculated rate constants for bicyclic isomerization of peroxy radicals are much faster than the first-order rate of competing reaction of peroxy radicals with NO in the atmosphere, which is only about 2 s⁻¹ assuming rate constant on the order of 10⁻¹¹ cm³ molecule⁻¹ s⁻¹ for the NO−peroxy radical reaction and an ambient NO mixing ratio of 10 ppb typical of a polluted urban atmosphere.[3,19−21] This conclusion is consistent with the literature work that suggests the aromatic peroxy radicals tend to bicyclic isomerization.[1,2,14] Note that the activation barriers for decomposition and isomerization of the peroxy radicals are nearly comparable, indicating competing pathways for the two channels (Table 3).

3.4. Epoxy Radicals and Bicyclic Peroxy Radicals. The fate of bicyclic radicals is isomerization or reaction with O₂. The high-lying transition states and unstable structures of the

nonallylic bicyclic radicals render formation of the majority of the epoxy radicals atmospherically irrelevant.[21] For the ipso OH addition, only the formation of epoxides EBPI is plausible, resulting from isomerization of BPI3. For the ortho OH addition, isomerization of the bicyclic radical BPO2 leads to two epoxides, i.e., EBP1 and EBP2. The equilibrium structures of those epoxides are shown in Figure 6, along with their corresponding transition states. At the transition states, the distances for breaking the O−O bond are 2.24 Å for all three epoxides, and the distances for C−O closure are 2.10, 2.11, and 2.13 Å for EBPI, EBP1, and EBP2, respectively. The relative stability of the epoxy radicals and the PES for bicyclic to epoxy radical isomerization are presented in Figure 5. The epoxy radicals are mostly noticeable for their high stability. The epoxides are about 15−17 kcal mol⁻¹ more stable than their corresponding bicyclic precursors (Table 2). For the ortho OH addition, the formed epoxide EBP1 is more stable than EBP2. The activation barrier to form EBPI from BPI3 is predicted to
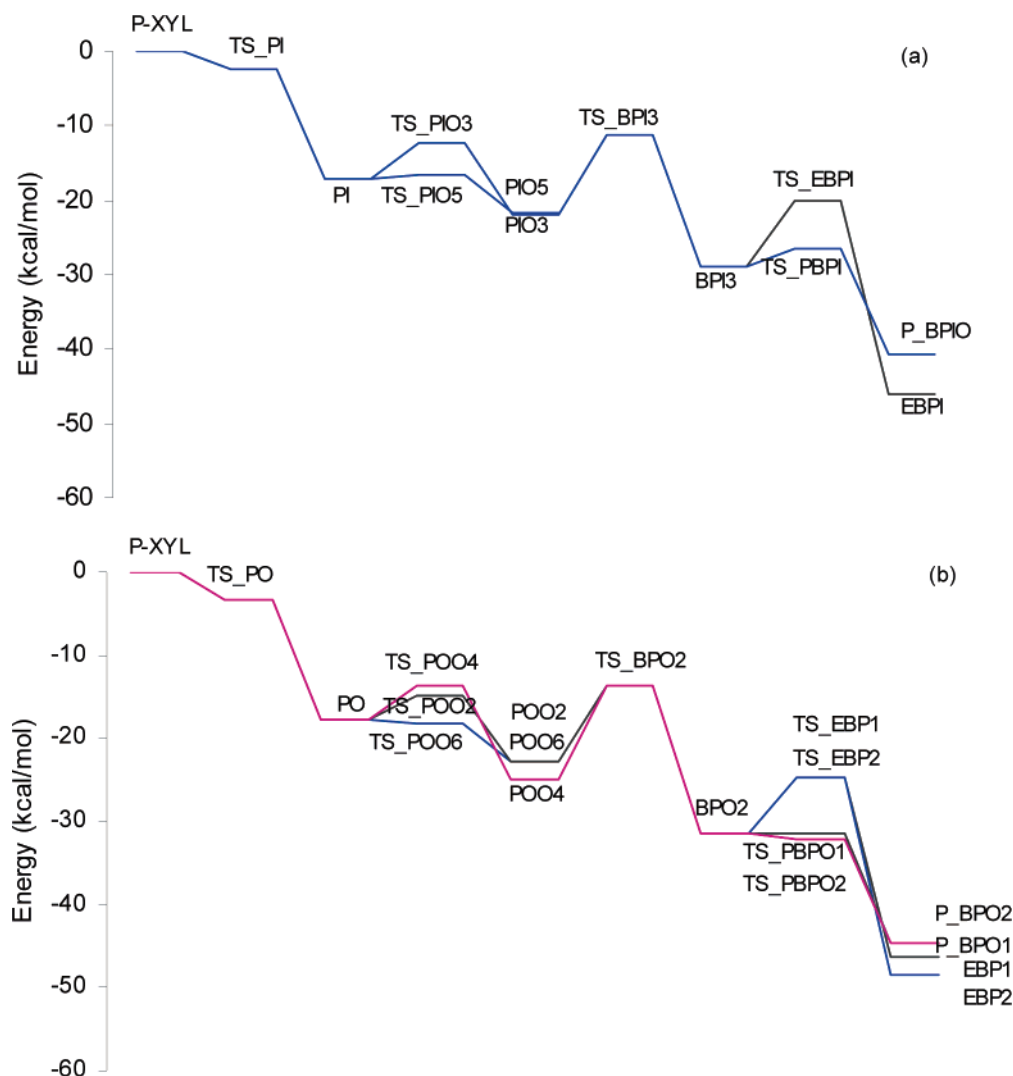
Figure 5. Overall potential energy surface (PES) of the *p*-xylene−OH reaction system: (a) for ipso OH addition; (b) for ortho OH addition.

be 8.8 kcal mol^{-1}. For the formation of EBP1 and EBP2, the activation barriers are about 7 kcal mol^{-1}. The calculated high-pressure limit rate constants for isomerization of the thermalized bicyclic radicals to epoxide are also shown in Table 3. Because of the high stability of the epoxides and low activation barriers, the calculated unimolecular rate constants to form the epoxides are relatively large, ranging from 10^6 to 10^7 s^{-1}. The calculated reversible rate constants are very small (10^{-4}–10^{-7} s^{-1}), suggesting that the isomerization reaction of the bicyclic radicals to epoxides occurs rapidly and irreversibly.

The bicyclic radicals also react with O$_2$ to form bicyclic peroxy radicals. For the ipso OH addition, only one bicyclic peroxy radical P_BPIO is possibly formed. For the ortho OH addition, the addition of O$_2$ to the different positions of the bicyclic radical BPO2 forms two possible bicyclic peroxy radicals P_BPO1 and P_BPO2. The equilibrium structures of those bicyclic peroxy radicals and their corresponding transition states are shown in Figure 7. At the transition states, the distances for forming the new C−O bond are 2.22, 2.27, and 2.38 Å for P_BPIO, P_BPO1, and P_BPO2, respectively. The PES for the bicyclic peroxy radicals is showed in Figure 5. The bicyclic peroxy radicals P_BPO1 and P_BPO2 are about 13 kcal mol^{-1} more stable than BPO2. Their activation barriers are very small, with the values of 0.2 and −0.7 kcal mol^{-1}, respectively, indicating small energy barriers for the formation of those two bicyclic peroxy radicals. The reaction and activation

energies of P_BPIO are comparable to those of P_BPO1 and P_BPO2, with the values of 14.2 and 2.4 kcal mol^{-1}, respectively. The binding energies of the bicyclic peroxy radicals are significantly larger than those of the corresponding primary peroxy radicals at the B3LYP/6-31G(d,p) level of theory. At the UHF/PM3//B3LYP/6-31G(d,p) level of theory, a barrier height of 5.5 kcal mol^{-1} for the formation of the bicyclic peroxy radical of *p*-xylene were obtained by Andino et al.,[13] notably different from our calculations at the B3LYP/6-31G(d,p)// B3LYP/6-31G(d,p) level. The calculated bimolecular rate constants for the formation of the bicyclic peroxy radicals range from 2.3×10^{-15} to 9.0×10^{-14} cm^3 molecule^{-1} s^{-1} (Table 3). O$_2$ addition to the bicyclic radical BPO2 to form P_BPO2 occurs about 4 times faster than that to form P_BPO1.

We now discuss the fate of the bicyclic radicals, i.e., the competition between isomerization to epoxides and O$_2$ addition to form bicyclic peroxy radicals. For both ipso and ortho addition pathways, isomerization of bicyclic radicals yields epoxide radicals which are slightly more stable than the bicyclic peroxy radicals (Figure 5). The effective first-order rate constants of the reactions of bicyclic radicals with O$_2$ are about 10^4–10^6 s^{-1}. Consequently, the O$_2$ addition rates to form the bicyclic peroxy radical are comparable to those of epoxide formation, indicating that both radicals are probably formed. The formed bicyclic peroxy radicals are then expected to react with NO to form the bicyclic alkoxy radicals and NO$_2$, which is important

Atmospheric Oxidation Mechanism of *p*-Xylene

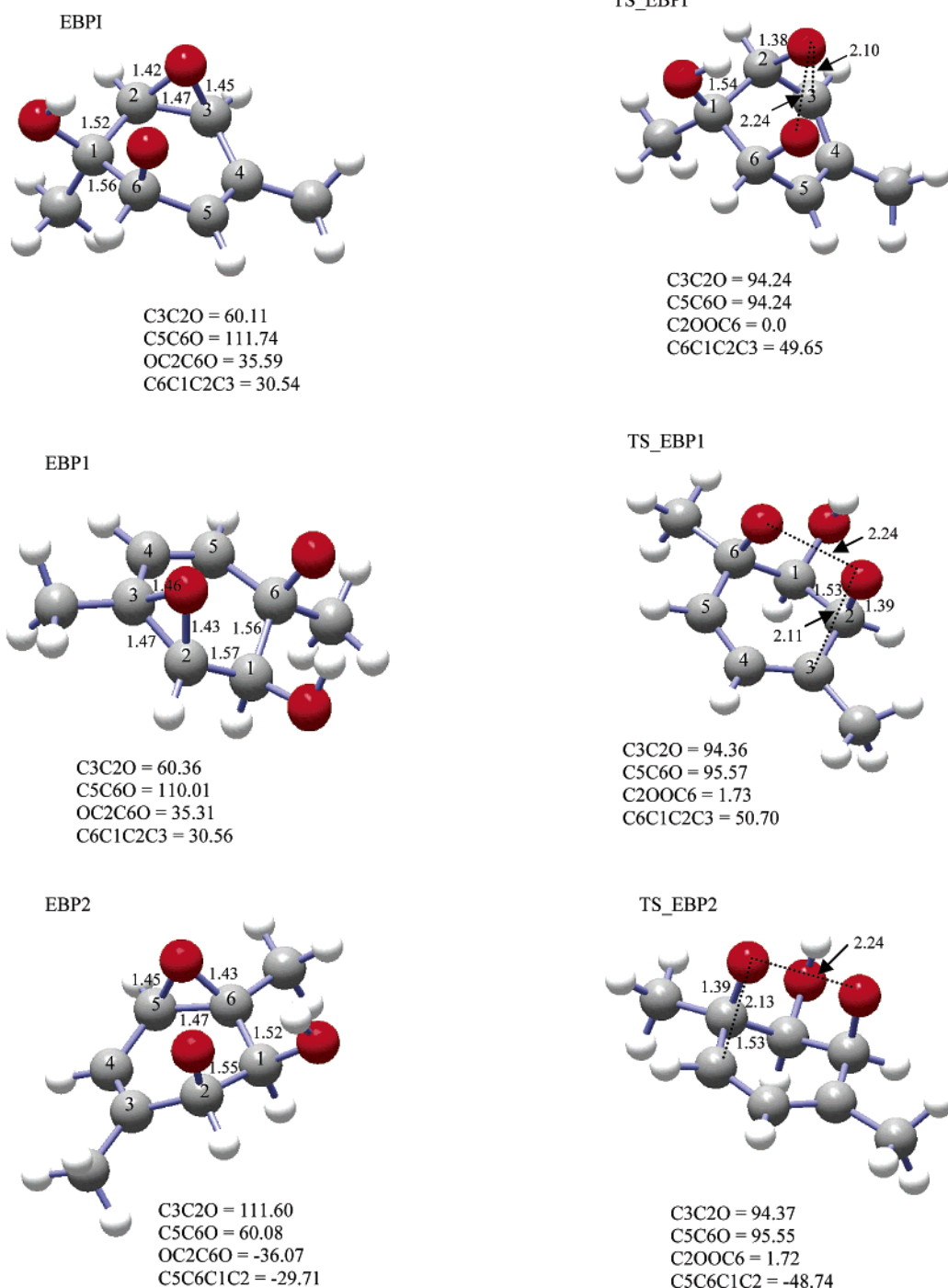*J. Phys. Chem. A, Vol. 110, No. 24, 2006* **7735**

Figure 6. Optimized geometries of epoxy radicals and their corresponding transition states at the B3LYP/6-31G(d,p) level of theory.

for ozone formation. The bicyclic alkoxy radicals subsequently undergo ring cleavage, leading to formation of glyoxal, methyl glyoxal, and several unsaturated anhydrides such as *cis*- and *trans*-3-hexene-2,5-dione which are the likely components of aerosols from the aromatics.[1,26,27] The large yields of the ring fragmentation products have been observed in experimental studies.[1,2,14] The formation of epoxides from the oxidation of toluene was suggested by Bartolotti and Edney in their theoretical calculations.[28] In the experiment study of the OH-initiated reactions of six alkylbenzenes using GC/MS detection, Jeffries and co-workers observed carbonyl products with their molecular weights matching a series of epoxide carbonyls.[4] Unlike the low possibility of formation of epoxides from the oxidation of benzene and toluene,[21,29] the formation of epoxides from the

oxidation of *p*-xylene is expected to be more probable since the energy barriers are low and the calculated rate constants are large, which may support the observation by Jeffries and co-workers who showed evidence of the formation of epoxide intermediates.[4] A most recent experimental study of *m*-xylene reactions with OH reported a small yet nonnegligible yield of 2−3% for the expoxy carbonyls.[30] Because of their potential toxicity and mutagenicity, the formation of the epoxide products may be a significant public health concern.

Conclusion

We have presented an investigation of the mechanistic features of OH-initiated oxidation reactions of *p*-xylene using
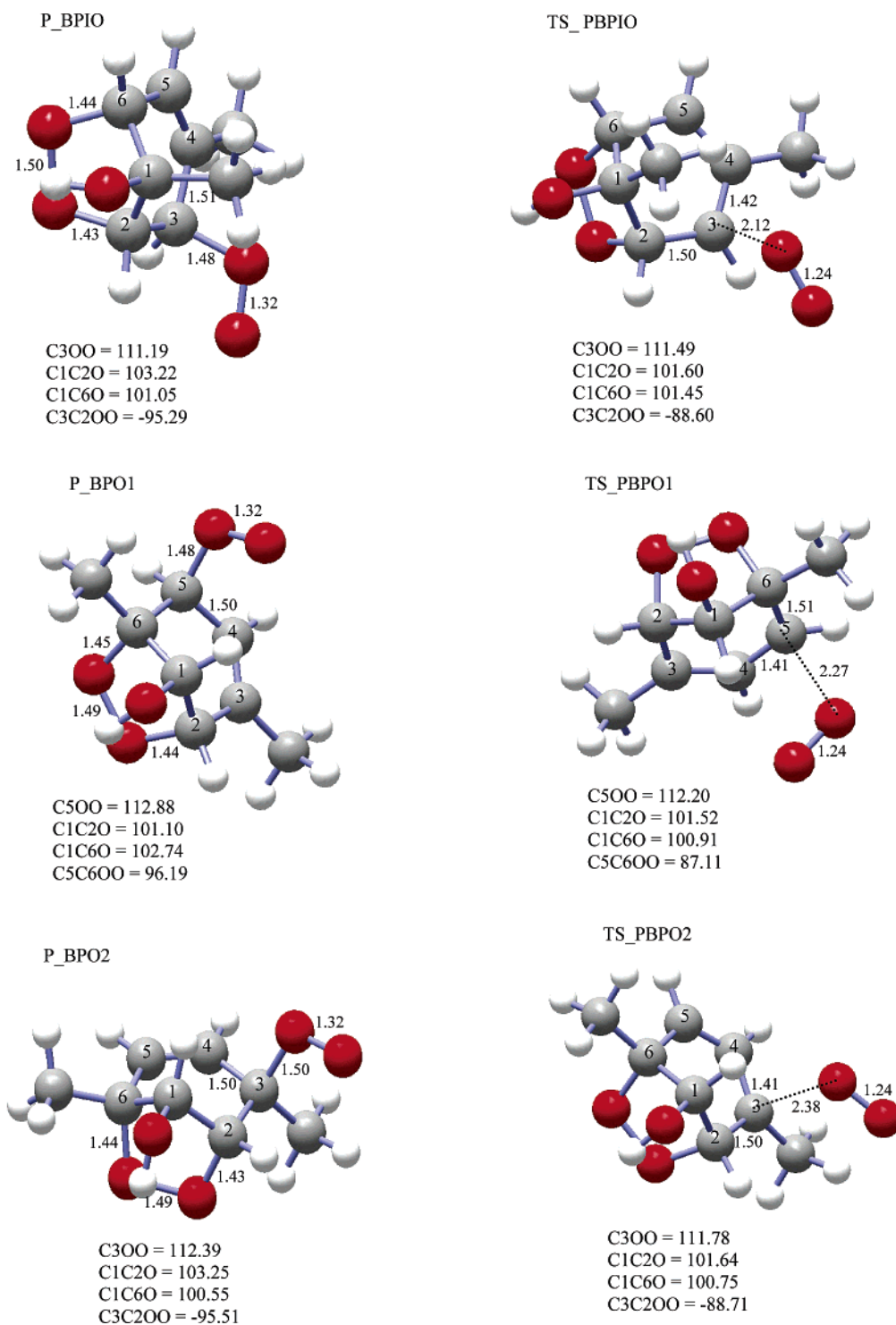
Figure 7. Optimized geometries of bicyclic peroxy radicals and their corresponding transition states at the B3LYP/6-31G(d,p) level of theory.

consistent density function theory (DFT). The study elucidates the reaction pathways for the atmospheric oxidation of *p*-xylene initiated by OH radicals. OH addition is predicted to occur dominantly at the ortho position, with the branching ratios of 0.8 and 0.2 for ortho and ipso additions, respectively. The calculated rate constant of *p*-xylene with OH is in agreement with available experimental studies. The results reveal that the *p*-xylene−OH−O$_2$ peroxy radicals preferentially cyclize to form bicyclic radicals under atmospheric conditions, rather than reacting with NO to lead to ozone formation, and that the back-decomposition to O$_2$ plus the hydroxyl *p*-xylene adduct is competitive with both processes, leading to a preequilibrium condition. With relatively low barriers, isomerization of the

p-xylene bicyclic radicals to more stable epoxide radicals likely occurs, competing with O$_2$ addition to form bicyclic peroxy radicals. In this work, we did not investigate the reaction pathways for H-abstraction from the methyl group of the *p*-xylene ring by OH and the likely fate of aromatic alkoxy radicals, which need to be addressed in further theoretical investigations.

Atmospheric Oxidation Mechanism of *p*-Xylene

J. Phys. Chem. A, Vol. 110, No. 24, 2006 **7737**

References and Notes

(1) Smith, D. F.; Kleindienst, T. E.; Mciver, C. D. *J. Atmos. Chem.* **1999**, *34*, 339−364.

(2) Hamilton, J. F.; Lewis. A. C.; Bloss, C.; Wagner, V.; Henderson, A. P.; Goldong, B. T.; Wirtz, K.; Martin-Reviejo, M.; Pilling, M. *J. Atmos. Chem. Phys. Discuss.* **2003**, *3*, 4359−4391.

(3) Seinfeld, J. H.; Pandis, S. N. *Atmospheric Chemistry and Physics: From Air Pollution to Climate Change*; John Wiley & Sons: New York, 1997.

(4) Yu, J.; Jeffries, H. E. *Atmos. Environ.* **1997**, *31*, 2281.

(5) Gery, M. W.; Fox, D. L.; Kamens, R. M.; Stockburger, L. *Environ. Sci. Technol.* **1987**, *21*, 339−347.

(6) Grosjean, D.; Fung, K. J. *Air Pollut. Control Assoc.* **1984**, *34*, 537−543.

(7) Lonneman, W. A.; Kopczynski, S. L.; Darley, P. E.; Sutterfield, F. D. *Environ. Sci. Technol.* **1974**, *8*, 229−236.

(8) ECO−USA, toxics: http://www.eco-usa.net/toxics/xylene.shtml.

(9) Molina, M. J.; Zhang, R.; Broekhuizen, K.; Lei, W.; Navarro, R.; Molina, L. T. *J. Am. Chem. Soc.* **1999**, *121*, 10, 225.

(10) Atkinson, R. *Atmos. Environ.* **1990**, *24*, 1−41.

(11) Perry, (r) A.; Atkinson, R.; Pitts, J. N. *J. Phys. Chem.* **1977**, *81*, 296−304.

(12) Knispel, R.; Koch, R.; Siese, M.; Zetzsch, C. *Ber. Bunsen-Ges. Phys. Chem.* **1990**, *94*, 1375.

(13) Andino, J. M.; Smith, J. N.; Flagan R. C.; Goddard, W. A.; Seinfeld, J. H. *J. Phys. Chem.* **1996**, *100*, 10967−10980.

(14) Volkamer, R.; Platt, U.; Wirtz, K. *J. Phys. Chem. A* **2001**, *105*, 7865−7874.

(15) Bandow, H.; Washida, N. *Bull. Chem. Soc. Jpn.* **1985**, *58*, 2541−2548.

(16) Hansen. D. A.; Atkinson, R.; Pitts, J. N. *J. Phys. Chem.* **1975**, *79*, 1763.

(17) Kwok, E. S. C.; Aschmann, S. M.; Atkinson, R.; Arey, J. *J. Chem. Soc., Faraday Trans.* **1997**, *93*, 2847−2854.

(18) Atkinson, R.; Aschmann, S. M. *Int. J. Chem. Kinet.* **1991**, *23*, 77−97.

(19) Calvert, J. G.; Atkinson, R.; Becker, K. H.; Kamens, R. M.; Seinfeld, J. H.; Wallington, T. J.; Yarwood, G. *The Mechanisms of Atmospheric Oxidation of Aromatic Hydrocarbons*; Oxford University Press: New York, 2002.

(20) Atkinson, R. *J. Phys. Chem. Ref. Data* **1997**, *26*, 215.

(21) Suh, I.; Zhang, R.; Molina, L. T.; Molina, M. J. *J. Am. Chem. Soc.* **2003**, *125*, 12655−12665.

(22) Suh, I.; Zhang, D.; Zhang, R.; Molina, L. T.; Molina, M. J. *Chem. Phys. Lett.* **2002**, *364*, 454.

(23) Zhang, D.; Zhang, R. *J. Am. Chem. Soc.* **2002**, *124*, 2692.

(24) Lei, W.; Zhang, R. *J. Phys. Chem.* **2001**, *105*, 3808.

(25) Fan, J.; Zhao, J.; Zhang, R. *Chem. Phys. Lett.* **2005**, *411*, 1.

(26) Forstner, H. J. L.; Flagan, R. C.; Seinfeld, J. H. *Environ. Sci. Technol.* **1997**, *31*, 1345.

(27) Zhang, R.; Suh, I.; Zhao, J.; Zhang, D.; Fortner, E. C.; Tie, X.; Molina, L. T.; Molina, M. J. *Science* **2004**, *304*, 1487.

(28) Bartolotti, L. J.; Edney, E. O. *Chem. Phys. Lett.* **1995**, *245*, 119.

(29) Motta, F.; Ghigo, G.; Tonachini, G. *J. Phys. Chem.* **2002**, *106*, 4411.

(30) Zhao, J.; Zhang, R.; Misawa, K.; Shibuya, K. *J. Photochem. Photobiol. A* **2005**, *176*, 199.